Chapter

Doping Effect on Piezoelectric, Magnetic and Magnetoelectric Properties of Perovskite—Ferromagnetic Magnetoelectric Composites

Rashed A. Islam

Abstract

This chapter explains the effect of compositional modification on the magnetoelectric coefficient in sintered piezoelectric – magnetostrictive composites. It was found that 15 at% doping of $Pb(Zn_{1/3}Nb_{2/3})O_3$ [PZN] in $Pb(Zr_{0.52}Ti_{0.48})O_3$ [PZT] enhances the piezoelectric and magnetoelectric properties of a PZT – 20 at% $Ni_{0.8}Zn_{0.2}Fe_2O_4$ [NZF] composite. The effect of doping on the ferromagnetic phase was also investigated. With increases in Zn concentration, it was found that the coercive field and Curie temperature of $Ni_{(1-x)}Zn_xFe_2O_4$ [NZF] decreases, while its saturation magnetization has a maxima at 30 mole% Zn. X-ray diffraction revealed that the lattice constant of NZF increases from 8.32 Å for 0 at% Zn to 8.39 Å for 50 at% Zn. The magnetoelectric coefficient was found to have a maxima of 144 mV/cm.Oe at 30 at% Zn. To understand better, the effect of 40% (by mole) Zn substitution on structural, piezoelectric, ferromagnetic and magnetoelectric properties of Pb $(Zr_{0.52}Ti_{0.48})O_3$ - $CoFe_2O_4$ (PZT - CFO) sintered composite is also explained. X-ray diffraction of $Co_{0.6}Zn_{0.4}Fe_2O_4$ (CZF) showed the shift in almost all diffraction peaks to lower diffraction angle confirming the increase in lattice parameter in all three direction from 8.378 (for CFO) to 8.395 Å for $(Co,Zn)Fe_2O_4$ (CZF). SEM and TEM results showed defect structure (cleavage, twins, strain fields) in the CZF particle, which is a clear indication of misfit strain developed due to lattice expansion. Magnetic properties measured over temperature (5 K – 1000 K) showed increased magnetization but lower magnetic Curie temperature in PZT - CZF particle. Magnetoelectric coefficient measured as function of ferrite concentration showed an increase of more than 100% after doping the CFO phase with 40% Zn. This enhancement can be attributed to increase in the lattice strain, magnetic permeability and decrease in coercivity.

Keywords: piezoelectric constant, dielectric constant, ferromagnetic, magnetoelectric coefficient, misfit strain

1. Introduction

Magnetoelectric [ME] particulate composites combine the magnetostrictive and the piezoelectric properties of materials, through product tensor properties [1].

Multiferroic magnetoelectric materials possess two or more ferroic properties such as ferroelectricity, ferromagnetism and ferroelasticity [2–4]. The spin lattice structure in a magnetoelectric composite can be directly related to (i) linear or non-linear shape change in magnetostrictive phase under alternative magnetic field, (ii) polarization change in piezoelectric phase through field induced alternating stress–strain and finally (iii) charge developed in the piezoelectric phase due to this alternating stress [1, 5, 6]. The interrelationship between ferroelectricity and magnetism allows magnetic control of ferroelectric properties and vice-versa. Single phase magnetoelectrics such as Cr_2O_3, $BiFeO_3$, $YMnO_3$ etc. exhibit poor combination of electric and magnetic properties at room temperature [7–9]. On the other hand, two-phase magnetoelectric (ME) materials provide large coupling and may play important role in future magnetoelectric devices [10]. Another important issue that can be very influential not only in nanostructures or multilayer structure but also in bulk ceramic composite is the interface chemistry. Migration of mobile atoms (from ferroelectric and magnetic phases) through the interface causes ferroelectric and magnetic instability and alters the interface chemistry, which affects the interface magnetoelectric properties [10, 11]. There are lot of advantages that sintered particulate offers, compared to in-situ composites (i.e. unidirectionally solidified of $BaTiO_3$ – $CoFe_2O_4$), such as they are cost effective to produce, fabrication is easy and finally and most importantly the process parameters can be controlled much better. In terms of ME responses, laminate magnetoelectric composites gained a lot of popularity and can be fabricated by attaching piezoelectric layer between two layers of magnetostrictive discs or plates. Sintered particulate composites exhibits low resistivity, defects, diffusions at the interface and incompatibility of elastic compliances and mismatch in coefficient of thermal expansion. As a result, sintered composites show inferior ME responses compared to laminated composites. Therefore, it is essential to augment the composition, grain size, grain orientation, and sintering conditions in order to enhance the Magnetoelectric properties of the sintered composites.

The composites exploit the product property of the materials [12–14] where the ME effect can be realized by mixing individual piezomagnetic and piezoelectric phases or individual magnetostrictive and piezoelectric phases. In early 70s, researchers at Philips Laboratories demonstrated ME composites [15–18] by unidirectional solidification of eutectic composition of $BaTiO_3$ – $CoFe_2O_4$. The results showed a high ME voltage coefficient dE/dH of 50 mV/cm•Oe with 1.5 wt % of excess of TiO_2 [15]. Later an even higher ME coefficient of 130 mV/cm•Oe was obtained in eutectic composition of $BaTiO_3$-$CoFe_2O_4$ by unidirectional solidification [17]. Currently, various particulate composites consisting of piezoelectric and magnetostrictive materials with different connectivity schemes including "3-0" and "2-0" have been reported, using $LiFe_5O_8$, $NiFe_2O_4$, $(Ni,Zn)Fe_2O_4$, $CoFe_2O_4$, $CuFe_2O_4$ as magnetostrictive materials and $BaTiO_3$, $Pb(Zr,Ti)O_3$ as piezoelectric phase [15–24].

The figure of merit for a ferromagnetic-ferroelectric composite is large magnetoelectric coefficient (i.e., susceptibility) given as:

$$\text{Figure or merit} = \sqrt{\mu\varepsilon}; \tag{1}$$

Here μ = ferromagnetic permeability and ε is the dielectric permittivity. It is eminent from Eq. (1) that a high dielectric constant piezoelectric phase and a high permeability magnetic phase would produce a composite with optimum ME response if we can keep the high resistivity, low interface defects and lower rate of interface diffusion. Literatures and experimental review showed that the Nickel

Ferrites are stable in PZT up to 1250°C and offers higher permeabilities. Also in terms of resistivity and loss, Ni based ferrite are preferable over Mn based ferrite, because Ni based Ferrites have higher electric resistivity and lower dielectric loss.

2. Principles of magnetoelectricity

The thermodynamic consideration of magnetoelectric effect is obtained from the expansion of free energy of the system in terms of magnetic and electric field, such as.

$$G\left(\vec{E},\vec{H}\right) = G_o - P_s\_E - M_s\_H - \frac{1}{2}\chi_{ij}(E)\_E_i\_E_j - \frac{1}{2}\chi_{ij}(H)\_H_i\_H_j - \alpha_{ij}\_E_i\_H_j \tag{2}$$

where and are the electric field and magnetic field respectively. Differentiation of Eq. (2) gives us polarization and magnetization as following:

$$P_i = -\left(\frac{\delta G}{\delta E}\right) = P_s + \chi_{ij}E_j + \alpha_{ij}H_j \tag{3}$$

$$M_i = -\left(\frac{\delta G}{\delta H}\right) = M_s + \chi_{ij}H_j + \alpha_{ij}E_j \tag{4}$$

Here α_{ij} is the magnetoelectric tensor. Magnetoelectric effect combines two important materials property, permittivity and permeability, and for a single-phase material they define the upper limit of α_{ij} as following.

$$\alpha_{ij} < \sqrt{\varepsilon_{ij}\mu_{ij}} \tag{5}$$

Single phase multiferroic materials shows either low permeability or low permittivity or both. As a result, the magnetoelectric coupling is small. For high response dual phase magnetoelectric materials, combination between ferroelectric and ferromagnetic phase need to be established via strain. Piezoelectric coefficient (d_{33}/d_{31}) defines the materials property that converts applied stress in to proportional electric charge. The linear equations for a piezoelectricity and magnetostrictions are given as:

$$D_3 = \varepsilon_{33}^T E_3 + d_{33}T_3 \tag{6}$$

$$S_3 = d_{33}E_3 + s_{33}^E T_3 \tag{7}$$

$$S = s^H T + qH \tag{8}$$

$$B = qT + \mu^T H \tag{9}$$

where
D = the dielectric displacement,
E = electric field,
T = stress,
S = strain,
ε = permittivity,
s = elastic compliance,
d = is piezoelectric charge constant.

B = magnetic induction.
q = piezo magnetic coefficient.
μ = permeability and.
H = magnetic field.

Magnetoelectric coefficient of a composite can be described in direct notation of tensors as:

$$T = cS - e^T E - \alpha S^{ms} \tag{10}$$

$$D = eS + \varepsilon E + \alpha H \tag{11}$$

$$B = \mu(\varepsilon, E, H)H \tag{12}$$

where σ, c and K are the stress, stiffness constant at constant field and dielectric constant at constant strain respectively. It was found in the literatures that ME coefficient can be varied by piezoelectric and piezomagnetic coefficients. Elastic compliances (s) of piezoelectric and magnetostrictive phases are found to be another critical parameter that affects the ME coefficient. According to Srinivasan et al., the ME coefficient can be written as:

$$\frac{\delta E_3}{\delta H_1} = \frac{-2d_{31}^p q_{11}^m v^m}{\left(s_{11}^m + s_{12}^m\right)\varepsilon_{33}^{T,P} v^p + \left(s_{11}^p + s_{12}^p\right)\varepsilon_{33}^{T,P} v^m - 2\left(d_{31}^p\right)^2 v_m} \tag{13}$$

where
d_{31}^p = piezoelectric coefficient,
v^m and v^p = volume of magnetic and piezoelectric phase,
t^m and t^p = thickness of magnetic and piezoelectric phase,
s_{11}^p, s_{12}^p = the elastic compliances for piezoelectric phase,
s_{11}^m, s_{12}^m = elastic compliances for magnetostrictive phase,
q_{11} = piezomagnetic coefficient of the magnetic phase and.
$\varepsilon_{33}^{T,P}$ = permittivity of the piezoelectric phase.

Further derivation for the magnetoelectric coefficient in T – T mode of Eq. (13) was done by Dong et al. and was expressed as:

$$\left|\frac{dV}{dH}\right|_{T-T} = \beta \frac{n(1-n)Ad_{33,m}d_{31,p}g_{31,p}}{S_{11}^E\left[nS_{11}^E\left(1-k_{31}^2\right) + (1-n)S_{11}^H\right]} \tag{14}$$

where
β = a constant related to DC magnetic field (<1),
n = the ratio of magnetostrictive layer thickness to the composite thickness,
d = the piezoelectric strain constant,
s = the elastic constant,
g = the piezoelectric voltage constant,
A = the cross-sectional area of the laminate and.
k = is the electromechanical coupling factor.

It is quite clear from the Eq. 14 that the ME coefficient is directly related to piezoelectric constant (d_{31}) and piezomagnetic coefficient (q_{11}). d_{31}^p which is related to dielectric permittivity [$d_{31}^2 = k_{31}^2\left(s_{11}^E \varepsilon_{33}^T\right)$] and q_{11} is related to permeability [$q_{11,m} = \mu_{33}.s_{33}.\lambda_{33}$].

3. Effect of doping

As is well known that compared to $BaTiO_3$, PZT has stronger piezoelectric and dielectric properties, higher Curie temperature, higher resistivity and lower sintering temperature. Doping in PZT can be done by adding acceptor dopants (Fe, Mn, Ni, Co) or donor dopants (La, Sb, Bi, W, Nb) in order to make it piezoelectrically hard or a soft. Hard piezoelectric materials can be characterized as decreased dielectric constant and loss, lower elastic compliance, lower electromechanical coupling factor, and lower electromechanical losses compared to undoped PZT. Soft piezoelectric materials exhibit increased dielectric constant, dielectric loss, elastic compliance, electromechanical coupling factor, and electromechanical losses. **Table 1** shows a comparison chart how the physical, dielectric and piezoelectric properties vary between soft and hard piezoelectric materials.

The open circuit output voltage (V), under an applied force of a ceramic is given as:

$$V = E \cdot t = -g \cdot X \cdot t = -\frac{g \cdot F \cdot t}{A} \tag{15}$$

where
t = the thickness of the ceramic,
E = the electric field, and.
g = the piezoelectric voltage coefficient given as:

$$g = \frac{d}{\varepsilon_o \varepsilon^X} \tag{16}$$

where ε^X is the dielectric constant under constant stress condition.
The charge (Q) generated on the piezoelectric ceramic is given by the relation:

$$Q/V = \frac{\varepsilon^X \varepsilon_o A}{t} = C \tag{17}$$

where

$$\text{C} = \text{the capacitance and} \tag{18}$$

Properties	Soft Piezoelectric	Hard Piezoelectric
Electrical Resistance	Higher	Lower
Permittivity	Higher	Lower
Dielectric Constants	Superior	Inferior
Dielectric Loss	Higher	Lower
Piezoelectric Constants	Superior	Inferior
Coercive Field	Lower	Higher
Mechanical Quality Factor	Lower	Higher
Electromechanical Coupling Factor	Larger	Smaller
Linearity	Poor	Better

Table 1.
Comparison of Dielectric and Piezoelectric properties between Soft and Hard Piezoelectric Materials.

It can be inferred from Eq. (17) that a piezoelectric plate can behave like a parallel plate capacitor at low frequencies. From here it can be derived that under ac stress, electric energy generated is given as:

$$U = \frac{1}{2}CV^2$$

or energy per unit volume,

$$u = \frac{1}{2}(d.g) \cdot \left(\frac{F}{A}\right)^2 \tag{19}$$

Eq. (15) and (19) conclude that under a fixed AC mechanical stress, piezoelectric material with high (d.g) product and high piezoelectric voltage (g) constant will generate high voltage and high power for a fixed area and thickness. In the case of magnetoelectric composite, the force is applied on the piezoelectric phase due to magnetostriction through elastic coupling, therefore the high energy density piezoelectric material will lead to higher response.

Nickel and cobalt ferrites have the advantage of higher resistivity and increased permeability. Cobalt ferrite has higher magnetization but also has higher coercivity compared to nickel ferrite. In order to increase the resistivity, permeability, and magnetization, doping of zinc in to ferrite is beneficial but it also reduces its magnetic Curie temperature. The theory behind this is, Zn^{+2} replaces Fe^{+3} on the tetrahedral sites as it is added to the spinel structure and Fe^{+3} occupies the vacant octahedral sites emptied by Co^{+2}. As a result, there will be no unpaired electrons for Zn^{+2}, Co^{+2} has one and Fe^{+3} has five. Hence the outcome of it is increase in magnetization of Zn-doped ferrites.

4. Synthesis and fabrication

$Pb(Zr_{0.52}Ti_{0.48})O_3$ (PZT), $0.85[Pb(Zr_{0.52}Ti_{0.48})O_3] - 0.15[Pb(Zn_{1/3}Nb_{2/3})O_3$ [PZT (soft)], $Pb(Zr_{0.56}Ti_{0.44})O_3 - 0.1\ Pb[(Zn_{0.8/3}\ Ni_{0.2/3})Nb_{2/3}]O_3 + 2$ (mol %) MnO_2 [PZT (hard)], $Ni_{(1-x)}Zn_xFe_2O_4$ [NZF] (where x varies from 0 to 0.5) and $Co_{(1-y)}Zn_yFe_2O_4$ [CZF], were synthesized using mixed oxide route. PZT, NZF and CZF powders were calcined at 750°C for 2 hrs and 1000°C for 5 hrs, respectively in order to make sure that inorganic oxides react to each other. Powder X-ray diffractions patterns were taken using Siemens Krystalloflex 810 D500 diffractometer to make sure that the pure perovskite and pure spinel structure was formed out of PZT/PZT (soft)/PZT (hard) and NZF/CFO/CZF. The PZT and NZF powders were then mixed together as 0.8 PZT – 0.2 NZF and compacted. CFO/CZF powders were mixed in PZT with stoichiometric ratio of 3, 5, 10, 15 and 20 mole percents. After homogeneous mixing using ball mill, powder was pressed using a hardened steel die having diameter of 12.7 mm under a pressure of 2 ksi and then cold isostatically pressed under pressure of 40 ksi. This was followed by pressure-less sintering in air at 1150°C for 2 hrs, resulting in consolidated ceramic composites. XRD patterns of sintered samples showed only two phases (PZT and CFO/CZF). Ag/Pd paste was painted manually on top and bottom of the sintered disc using a paint brush and heated for an hour at 825° C. The polarization process was done in a heated (120°C) silicone oil bath. D.C. electrical field of 2.5 kV/mm for 20 minutes was applied for the poling process. Dielectric constant as a function of temperature was measured using HP 4274A LCR meter (Hewlett Packard Co. USA). Magnetization as a function of temperature was measured using Quantum Design physical properties

measurement system from room temperature to 900 K. Transmission electron microscopy (TEM) was conducted by using JEOL 1200EX machine with an accelerated voltage of 120 kV.

5. Results and discussions

Figure 1(a) [25] Compares the polarization of undoped, hard and soft PZT. The max polarizations observed were 14.61, 23.54 and 31.65 μC/cm^2 respectively for these three groups. It was also recorded that elastic compliance (S_{11}) of these three compositions are 1.74 x 10^{-11} (soft), 1.37 x 10^{-11} (hard) and 1.11 x 10^{-11} (undoped) m^2/N respectively. Due to the presence of metal vacancies, soft PZT's have higher polarizations per unit field applied, resulting in enhancement in both the dielectric and the piezoelectric susceptibilities.

An increase in piezoelectric constant (d_{33}) (from 75 to 105 pC/N) and increase in dielectric constant (from 642 to 914) was observed when an undoped PZT was doped with PZN to make it soft. These increase in dielectric and piezoelectric properties clearly reflected in Magnetoelectric coefficient of PZT (soft) – 20 NZF composite $\frac{\delta E}{\delta H}$ = 186.5 mV/cm.Oe. as observed in **Figure 1(b)**. Due to increase in electromechanical coupling, smaller coercive field, and superior dielectric and piezoelectric properties Soft PZTs show larger ME voltage coefficient compared to hard (154 mV/cm.Oe) or undoped PZT (128 mV/cm.Oe).

Microstructure of PZT (undoped) – 20NZF and PZT (soft) – 20NZF composites were dense with the measured densities of ≥95% [25]. And the average grain size of the PZT – 20NZF composite was about 800 - 850 nm, whereas that of PZT (soft) – 20 NZF was smaller and the average ranges between 650 and 700 nm. Doping of PZN in PZT reduces the grain size as both the composite were sintered at 1150°C for 2 hours. In one of our previous studies it was shown that above 600 nm, the ME coefficient does not change much with increase in grain size [26]. So, both PZT (undoped) – 20NZF and PZT (soft) – 20NZF composites have optimum grainsize in terms of ME coefficient. Besides the grainsize reduction, the resistivity of PZT increases upon doping with PZN, as lower leakage currents were observed after poling (**Figure 2**).

Figure 3 [25] shows the saturation magnetization (M_s), coercive field (H_c) and magnetic Curie Temperature of the PZT – 20NZF composite as a function of Zn doping in NZF. It is clearly observed that the coercive field starts to drop as we increase the Zn doping in NZF. On the other hand, saturation magnetization becomes optimum (0.72 emu/gm) at around 30% Zn doping in NZF and then starts

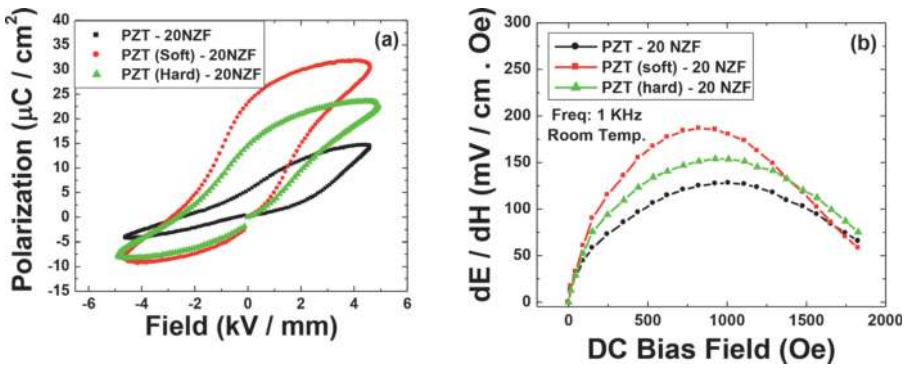

Figure 1.
(a) Polarization vs. electric field loop and (b) ME coefficient vs. DC bias of different compositions of PZT – 20 NZF composites [25].

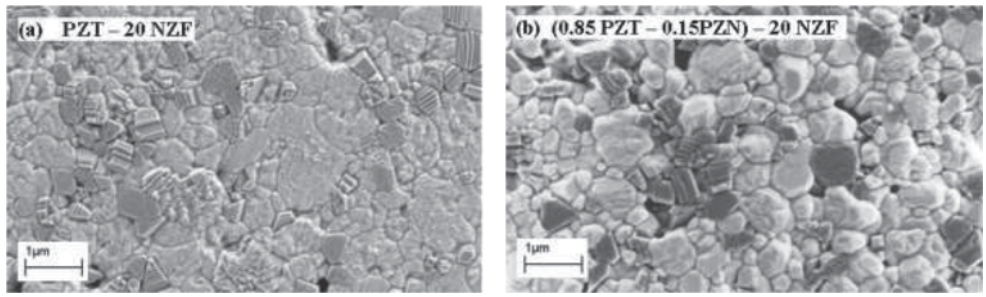

Figure 2.
Microstructure of (a) PZT – 20 NZF and (b) (0.85PZT –0.15 PZN) – 20 NZF [25].

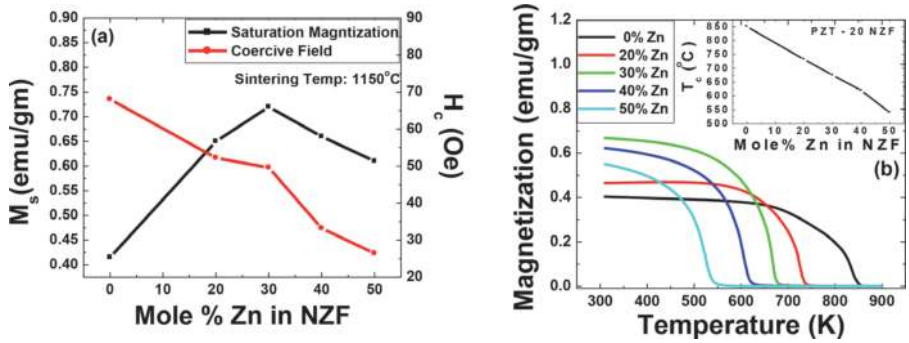

Figure 3.
Magnetic properties as a function of Zn doping. (a) M_s and H_c vs. Zn concentration and (b) magnetization vs. temperature [25].

to drop off with increase in Zn doping. In terms of Ferromagnetic Curie Temperature, it started to drop from 850 K to 549 K as the Zn concentration was increased from 0 to 50 mole %.

Figure 4(a) [25] Shows the hkl = (400) diffraction peak for NZF composites as a function of Zn concentration. The (400) peak started to shift towards lower Bragg angles as Zn concentration was increased which indicated an enlargement of lattice parameters. From Bragg's law, we determine a 0.9% lattice expansion (8.32 Å for $NiFe_2O_4$ and 8.394 Å for $Ni_{0.5}Zn_{0.5}Fe_2O_4$) with this change in crystal chemistry. **Figure 4(b)** shows the ME voltage coefficient as a function Zn concentration in PZT – 20 NZF. 30 at% Zn concentration in NZF showed the maximum value of $\frac{\delta E}{\delta H}$ = 138 mV/cm.Oe, whereas 0 at% Zn concentration in NZF (pure Ni ferrite) has a

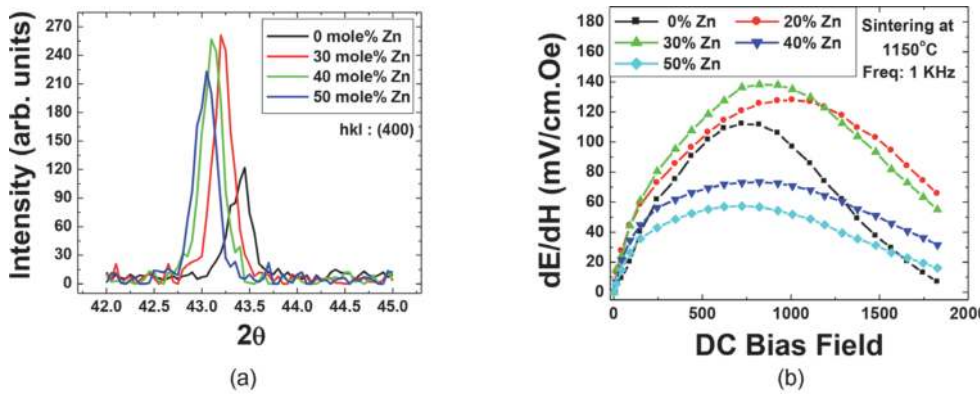

Figure 4.
Effect of Zn concentration on (a) peak shift of 400 peaks and (b) magnetoelectric coefficient of PZT – 20 NZF [25].

maximum value of 112 mV/cm.Oe. With Zn concentration above 30%, the ME coefficient dropped notably, reaching a value of 60 mV/cm.Oe for 50 at% Zn. Saturation magnetization and magnetoelectric responses as a function of Zn concentration in NZF was found to have similar effect because permeability μ is directly related to magnetization M, via $\mu = 1 + 4\pi\frac{M}{H}$. Furthermore, the changes in the ME coefficient with Zn concentration depends on the change in effective piezomagnetic coefficient ($d_{33,m} = \mu_{33}.s_{33}.\lambda_{33}$) which is directly related to the permeability.

Figure 5 (a-c)show the density, dielectric constant and piezoelectric constant as a function of mole percent ferrite in the composite for two different compositions. It is clear that as the ferrite concentration increases, density, dielectric constant and piezoelectric constant decreases. All the compositions showed more than 98% of the theoretical density and the microstructural analysis confirmed this measurement. For PZT – CFO, there is a slight increase in density from 3–5% concentration which can be attributed to better sintering as the.

ferrite becomes more homogenized in the matrix. The density increase was also observed when the composition changed from 10–15% for CFO in PZT – CFO composite. This can be explained by grain coarsening of PZT. As the CFO content increases from 10–15% there is slight increase in dielectric constant and then with further increase in ferrite concentration, dielectric constant starts to drop. It is well-known that grain coarsening has direct effect on dielectric properties, whereby, dielectric constant increases with larger grain size. There was no significant difference in piezoelectric data between CFO and CZF based ferrite composites with ferrite concentration.

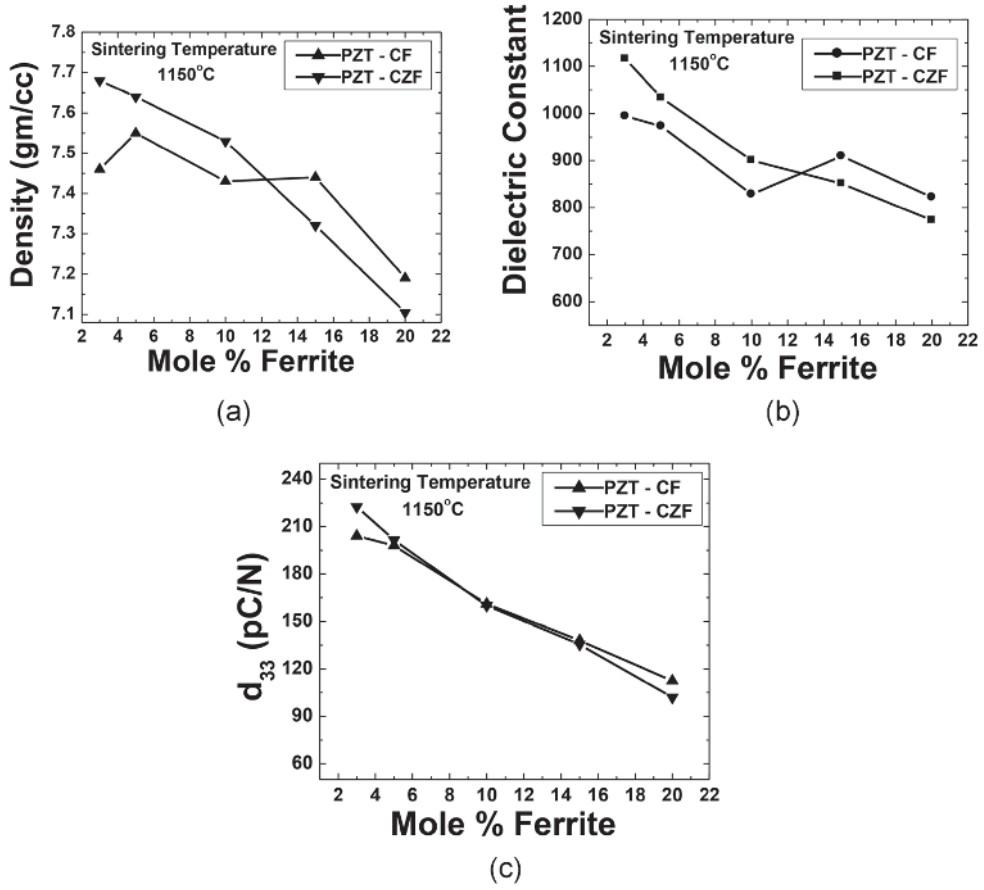

Figure 5.
(a), (b) and (c) The density, dielectric constant and piezoelectric constant as a function of mole percent ferrite.

A comparison between PZT – CFO and PZT – CZF in terms of room temperature magnetic properties is presented in **Figure 6(a)** and **(b)** for 3% and 5% ferrite concentration. In both the cases, a considerable difference in coercivity between CFO and CZF particles was observed. For 3% ferrite concentration the saturation magnetization of CFO was slightly higher than CZF but the coercivity was much lower (33 Oe compared to 263 Oe). For 5% CFO and CZF concentration, coercive fields of 53 and 288 Oe were measured and the saturation magnetization of CFO particle (76.6 memu) was slightly lower than the CZF particle (88.54 memu). **Figure 6(c)** and **(d)** show the magnetization of PZT – 5 CFO and PZT – 5 CZF composites from 5 K to 300 K and from 310 K to 1000 K respectively. It is quite interesting to observe that the magnetization for both the composites start to drop from 5 K to 300 K. The drop for PZT – 5CFO is linear - 0.04 emu to 0.035 emu and for PZT – 5CZF is non –linear 0.075 to 0.065 emu respectively for 70 mg of sample weight. There is a slope change in the PZT – CZF magnetization curve at around 150 K – which is close to the curie temperature of $ZnFe_2O_4$. From 150 K to 5 K – an increased slope was observed. Below the curie temperature, Zn ferrite also contributed to the magnetization curve. Besides the increase in magnetization in subzero temperature for both the composites can also be explained by the atomic vibration of the crystal lattice. As the temperature starts to drop below the room temperature and approaches the absolute zero temperature, the atomic vibration is seized, resulting in much stable crystal lattice, which gives us accurate measurement of the magnetization. At high temperature (from 310 to 1000 K) the magnetization of PZT – CFO starts to increase and then decrease to zero at Curie temperature, which is almost 750 K. The PZT – CZF Curie temperature was recorded at 450 K. This drop

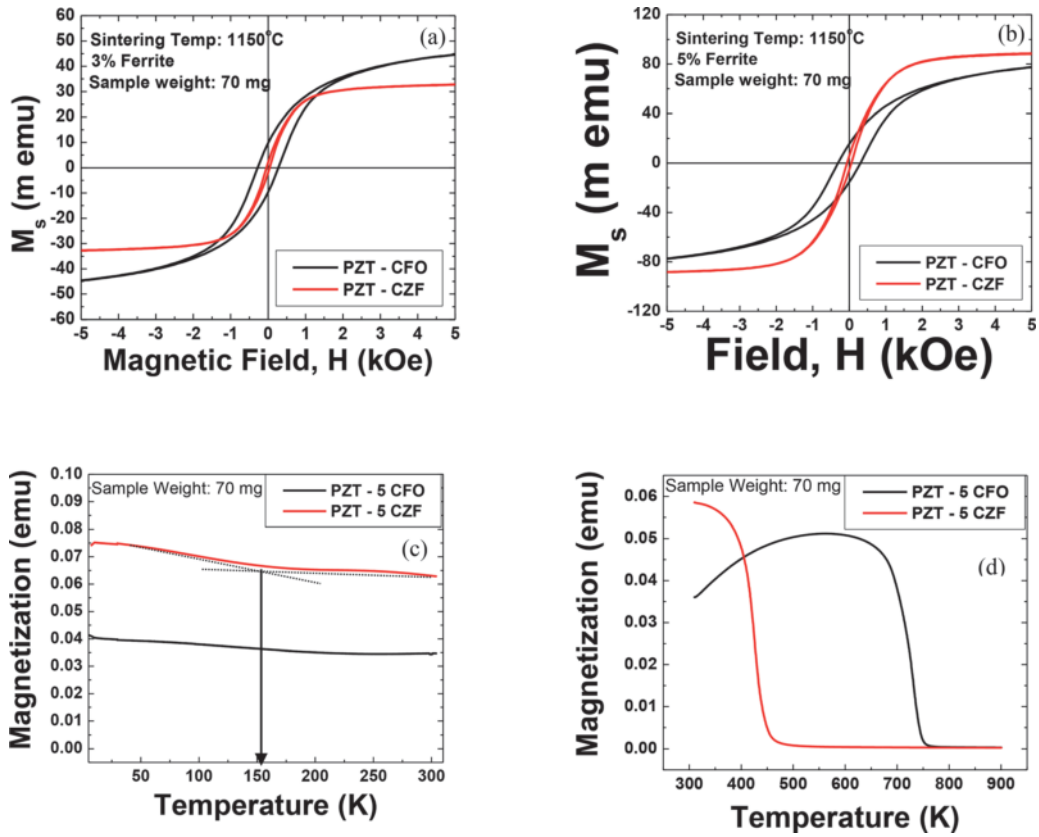

Figure 6.
(a) and (b). Hysteresis loop for PZT – CFO and PZT – CZF. (c) and (d): the magnetization of PZT – 5 CFO and PZT – 5 CZF composites.

in Curie temperature from 750 to 450 K is due to the substitution of Zn on the cobalt site. The substitution of Zn^{2+} for Fe^{3+} reduces the Curie temperature of the ferrite [6, 7, 9]. On the other hand, increasing the zinc content of cobalt-zinc ferrites increases their lattice parameter while decreasing the saturation magnetization above 50% Zn due to augmented B-B interaction followed by reduced A-B interaction. Also, the presence of Co^{2+} ion in the cobalt-zinc ferrite hastens the $Co^{2+} + Fe^{3+} \Leftrightarrow Co^{3+} + Fe^{2+}$ exchange reaction in octahedral sites, while tetrahedral sites are preferentially occupied by zinc cations. Tetrahedral sites in the spinel structure are suitable for cationic radii in the range of 0.58 Å to 0.67 Å, while octahedral sites can accept cations with radii in the range of 0.70 Å to 0.75 Å [22]. Therefore, in the unit cell structure, Co^{2+} (0.72 Å) and Fe^{2+}(0.75 Å) may replace Zn^{2+}(0.74 Å), while Co^{3+}(0.63 Å) can exchange sites with Fe^{3+}(0.64 Å). This exchange in Co-Zn ferrite system, the substitution of non-magnetic zinc in place of ferromagnetic cobalt leads to a decrease in Curie temperature owing to diminishing A-B super exchange interaction.

Figure 7 shows the XRD pattern for CFO and CZF particles. Inset shows magnified 311 peaks for CFO and CZF particles respectively. The shift in peaks to lower angle for CZF particles is clearly noticeable which results in a larger unit cell size for CZF particles. The increase in unit cell can induce strain. Strain can be revealed as strain fields or cleavage or other defects inside the microstructure. **Figure 8** shows the ME coefficient as a function.

of ferrite concentration. For PZT – CFO the maximum ME coefficient of 25 mV/cm.Oe was recorded at 15% ferrite concentration, which drops again for 20% ferrite. The measured ME coefficient is quite low compared to the PZT – Nickel ferrite composites. Cobalt ferrite has a very high coercive field compared to the nickel ferrite composition. Thus, a high DC bias field is necessary to obtain the peak ME coefficient. Another contributing factor is the initial permeability. Cobalt ferrite has lower initial permeability than the nickel ferrite which contributes towards lower ME coefficient.

Figure 9(a) and **(b)** show the SEM images of the microstructure of the PZT-20CFO and PZT – 20CZF samples sintered at 1125°C respectively. Dense microstructures for both compositions were obtained and the sintered samples had grain size of 1 to 1.5 μm. Elemental analysis using the EDX showed that CFO and CZF

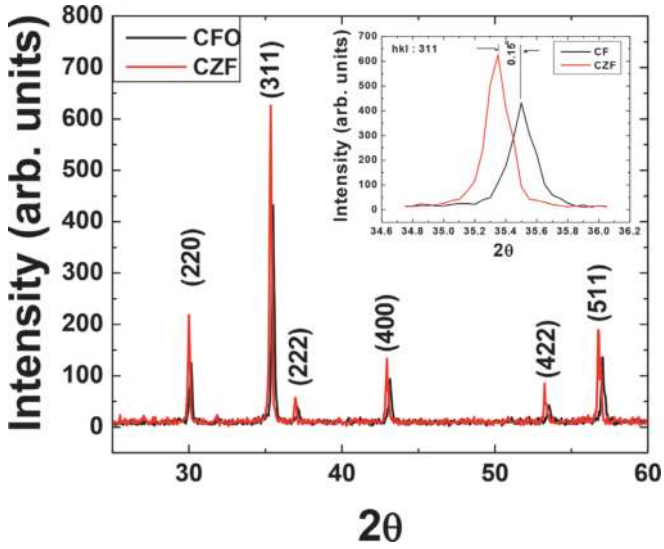

Figure 7.
XRD patterns for CFO and CZF particles.

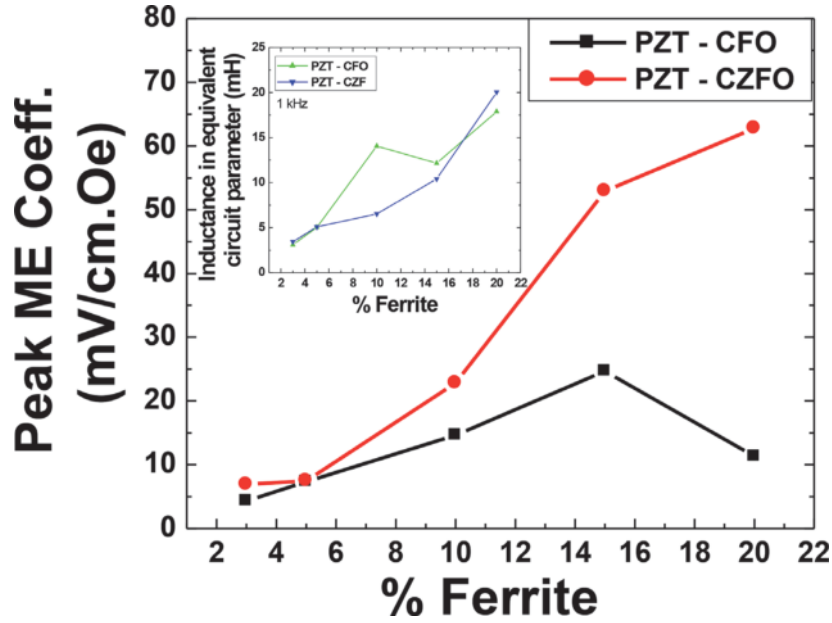

Figure 8.
ME coefficient as a function of ferrite concentration.

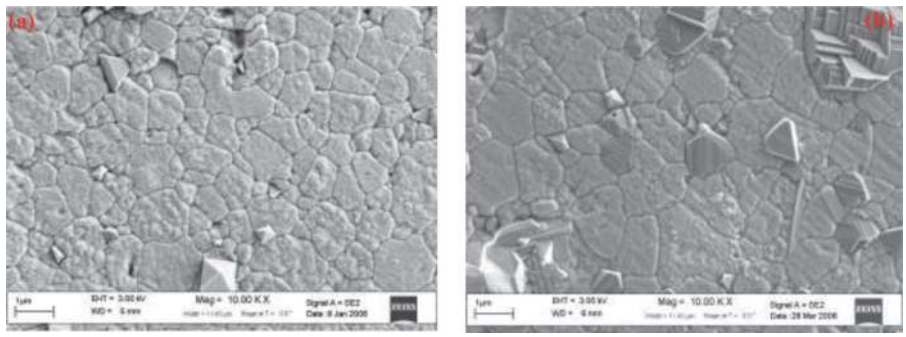

Figure 9.
(a) and (b): SEM images of the microstructure of the PZT-20CFO and PZT – 20CZF.

grains are distributed in the piezoelectric matrix. **Figure 10(a)** and **(b)** shows the bright field TEM images of the sintered.

PZT – 20 CFO and PZT – 20 CZF samples respectively. Compared to PZT – CFO, PZT - CZF sintered samples were found to consist of twin boundaries, cleavage, and strain fields at the interface of PZT and CZF grains. These defects develop to accommodate the mismatch in the PZT and CZF lattices, as ferrite (CFO/CZF) lattice parameters are more than double the lattice parameter of the PZT lattice. The lattice parameter increases by 0.2% for 40% Zn doped sample as observed in the XRD patterns. In the inset, diffraction pattern of a PZT grain is shown. No superlattice diffraction spots were observed near the first order diffraction spots, which indicate less intense diffusion level. From the SAED diffraction pattern the lattice parameter a and c are calculated as 4.05 and 4.132 Å, hence the c/a ratio is 1.02. Larger width domain patterns were also observed near the interface, which is characteristic of 90° domains. Besides that, intergranular heterogeneity in domain width is observed all over the structure especially near the interface. The observed defects in PZT - 5% CZF are in line with the SEM images. A finer scale domain structure, which usually has striation like morphology and periodically spaced was

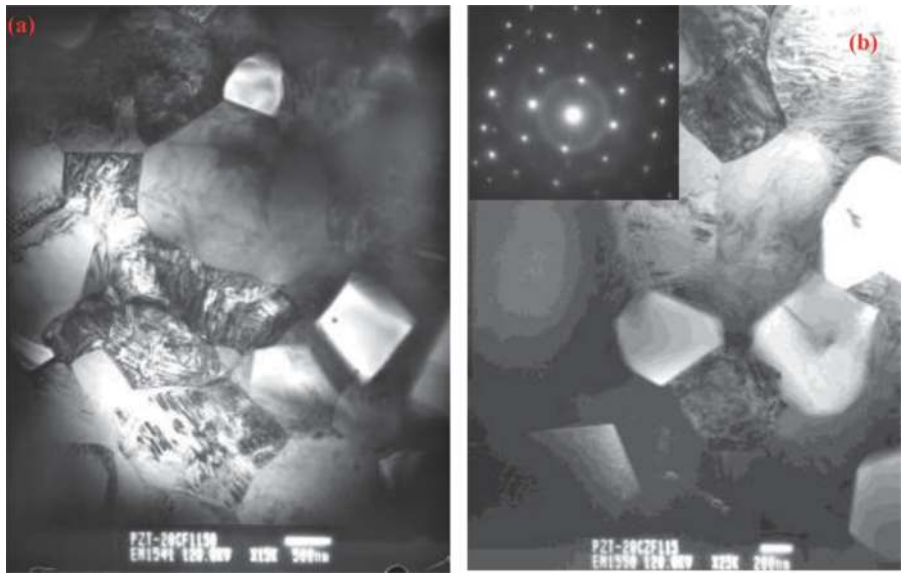

Figure 10.
(a) and (b): bright field TEM images of the sintered PZT – 20 CFO and PZT – 20 CZF.

observed in this structure away from the interface. These finer domains appear when the stress is relieved from the structure. It can be inferred that near the ferroelectric – ferromagnetic interface, the stress is higher and defects are observed due to strain mismatch, whereas the area away from the interface has lower stress.

6. Conclusion

In summary, it is understood from the experimental studies that the magnetoelectric coefficient ($\frac{\delta E}{\delta H}$) of a composite can be increased, using individual phases with higher piezoelectric and higher magnetization values. It was found that the soft piezoelectric phase can increase the ME value and higher Zinc doping was found to improve the magnetoelectric response of PZT – CFO based magnetoelectric composite. The coercive field of the CZF particles was lower than the CFO particles, which contributes towards the easy reversal of magnetic domain under AC magnetic field. The addition of Zn, contributes to the increase in saturation magnetization and hence the permeability. It has already reported that with high magnetic permeability inside the ferromagnetic material, magnetic flux strength increases and hence it helps to increase the effective piezomagnetic coefficient ($d\lambda/dH$). This increase in piezomagnetic coefficient helps to improve the magnetoelectric coefficient of the composites.

Acknowledgements

I would like to thank Prof. Shashank Priya of Penn State University for his technical guidance.

Author details

Rashed A. Islam
Alphabet Inc., 1600 Amphitheatre Parkway, Mountain View, CA 94043, USA

*Address all correspondence to: rashed_ms@yahoo.com

References

[1] Hur N, Park S, Sharma PA, Ahn JS. S. Guha and S-W Cheong. Nature. 2004; **429**:392

[2] Wang J, Zheng H, Lofland SE, Ma Z, Ardabili LM, Zhao T, et al. Science. 2004;**303**:661

[3] Ederer C, Spaldin N. Nature Materials. 2004;**3**:849

[4] Eerenstein W, Mathur ND, Scott JF. Nature. 2006;**442**:759

[5] Kimura T, Goto T, Shintani H, Ishizaki K, Arima T, Tokura Y. Nature. 2003;**426**:55

[6] Lottermoser T, Lonkal T, Amann U, Hohlwein D. J. Ihiringer and M. Fiebig. 2004;**430**:541

[7] Astrov DN. Sov. Phys. JETP. 1960;**11**: 708

[8] Wang J, Neaton JB, Zheng H, Nagarajan V, Ogale SB, Liu B, et al. Science. 2003;**299**:1719

[9] Van Aken BB, Palstra TTA, Filippetti A, Spaldin NA. Nat. Mater. 2004;**3**:164

[10] Duan CG, Jaswal SS, Tsymbal EY. Phys. Rev. Lett. 2006;**047201**:97

[11] Fiebig M, Lottermoser T, Frohllch D, Goltsev AV, Pisarev RV. Nature. 2002;**419**:818

[12] Zheng M, Wan JG, Wang Y, Yu H, Liu JM, Jiang XP, et al. J. Appl. Phys. 2004;**95**(12):8069

[13] Ryu J, Carazo AV, Uchino K, Kim H. J. Of Electocer. 2001;**7**:17

[14] Flores VC, Baques DB, Flores DC, Aquino JAM. J. Appl. Phys. 2006;**99**: 08J503

[15] Boomgaard JVD. A.M.J.G. Van Run and J.V Suchtelen. Ferroelectrics. 1976; **10**:295

[16] Boomgaard JVD, Born RAJ. J. Mater. Sci. 1978;**13**:1538

[17] Boomgaard JVD, Terrell DR, Born RAJ, Giller HFJI. J. Mater. Sci. 1974;**9**:1705

[18] Van Run AMJG, Terrell DR, Scholing JH. J. Mater. Sci. 1974;**9**:1710

[19] Lupeiko TG, Lisnevskaya IV, Chkheidze MD, Zvyagintsev BI. Inorg. Mater. 1995;**31**:1139

[20] T. G.Lupeiko, I. B.Lopatina, SS Lopatin, and IP Getman. Neorg. Mater. 1991;**27**(11):2394

[21] Lupeiko TG, Lopatina IB, Kozyrev IV, Derbaremdiker LA. Neorg. Mater. 1991;**28**(3):632

[22] Bokhan YI, Laletin VM. Inorg. Mater. 1996;**32**(5):634

[23] TG Lupeiko, SS Lopatin, IV Lisnevskaya, and BI Zvyagintsev, Inorg. Mater., 30, 1353, (1994).

[24] Dai YR, Bao P, Zhu JS, Wan JG, Shen HM, Liu JM. J. Appl. Phys. 2004; **96**(10):5687

[25] Islam RA, Priya S. J of Mat. Sci. 2008;**43**(4):1497-1500

[26] Islam RA, Priya S. J of Mat. Sci. 2008;**43**(10):3560-3568